On concentration polarisation in a fluidized bed membrane reactor for biogas steam reforming: Modelling and experimental validation

Niek de Nooijer[a], Fausto Gallucci[a,*], Emma Pellizzari[a,b], Jon Melendez[c],
David Alfredo Pacheco Tanaka[c], Giampaolo Manzolini[b], Martin van Sint Annaland[a]

[a] *Chemical Process Intensification, Department of Chemical Engineering and Chemistry, Eindhoven University of Technology, De Rondom 70, 5612 AZ Eindhoven, The Netherlands*
[b] *Department of Energy, Politecnico di Milano, via Lambruschini 4, 20156 Milano, Italy*
[c] *Tecnalia Energy and Environment Division, Mikeletegi Pasealekua 2, 20009 San Sebastian-Donostia, Spain*

HIGHLIGHTS

- Fluidized bed reactor model accounting for concentration polarization.
- Reduction of concentration polarization in fluidized bed is demonstrated.
- Experimental demonstration and model validation of biogas steam reforming in a FBMR.
- The H_2 productivity is proportionally related to the concentration polarization.

ARTICLE INFO

ABSTRACT

The production of pure hydrogen through the steam reforming of biogas in a fluidized bed membrane reactor has been studied. A phenomenological one-dimensional two-phase fluidized bed reactor model accounting for concentration polarisation with a stagnant film model has been developed and used to investigate the system performance. The validation of the model was performed with steam reforming experiments at temperatures ranging from 435 °C up to 535 °C, pressures between 2 and 5 bar and CO_2/CH_4 ratios up to 0.9. The permeation performance of the ceramic-supported PdAg thin-film membrane was first characterized separately for both pure gas and gas mixtures. Subsequently, the membrane was immersed into a fluidized bed containing Rh supported on alumina particles and the reactor performance, viz. the methane conversion, hydrogen recovery and hydrogen purity, was evaluated under biogas steam reforming conditions. The resulting hydrogen purity under biogas steam reforming conditions was up to 99.8%. The model results were in very good agreement with the experimental results, when assuming a thickness of the stagnant mass transfer boundary layer around the membrane equal to 0.54 cm. It is shown that the effects of concentration polarisation in a fluidized bed membrane reactor can be well described with the implementation of a film layer description in the two-phase model.

1. Introduction

The increasing energy demand over the last decades, in combination with the need to reduce greenhouse gas (GHG) emissions, has given rise to the development of more efficient conversion technologies and alternative energy carriers. Hydrogen is the most promising energy carrier, as it can be produced from renewable energy sources and no CO_2 is emitted at the end user. Most of the hydrogen produced nowadays is made via steam reforming of natural gas, producing significant GHG emissions. The current demand for hydrogen and its potential use in the new energy systems requires the development of a sustainable route for its production. Biogas is one of the renewable sources that could be used in the production of hydrogen.

Biogas is produced from biomass, which consists of organic matter (that captured carbon form atmospheric CO_2 over a relatively short timescale), mainly through anaerobic digestion of organic substrates (manure, sewage sludge, organic fractions of industry waste and energy crops) [1]. The composition of biogas varies significantly depending on the source of biomass. Typical biogas compositions from an anaerobic digester and landfill production are shown in Table 1.

The methane in the biogas can be converted into a hydrogen rich gas by steam reforming (SR): methane reacts with steam at high

Nomenclature

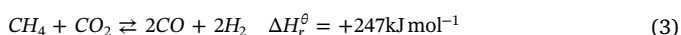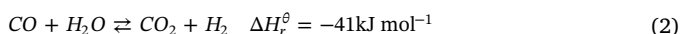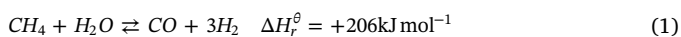|	
Ar	Archimedes number
A_j	Arrhenius pre-exponential factor
A_T	Area of bed cross section [m^2]
$d_{b,0}$	Initial bubble diameter [m]
d_b	Bubble diameter [m]
$d_{b,avg}$	Average bubble diameter [m]
$d_{b,max}$	Maximum bubble diameter [m]
d_p	Particle diameter [m]
D_g	Gas diffusivity [m^2 s^{-1}]
D_T	Bed diameter [m]
$E_{act,j}$	Activation energy for reaction j
f_k	Fraction of phase k
F_i	Molar flow of species i [mol s^{-1}]
g	Gravitational acceleration [m s^{-2}]
H_{mf}	Height of the bed at minimum fluidization velocity [m]
H_f	Height of the fluidized bed [m]
H_s	Height of the packed bed [m]
K_{ce}	Volumetric interchange coefficient between cloud and emulsion [s^{-1}]
K_{bc}	Volumetric interchange coefficient between bubble and cloud [s^{-1}]
$K_{be,i,n}$	Volumetric interchange coefficient between bubble and emulsion phase [s^{-1}]
K_j^{eq}	Equilibrium constant for reaction j
$M_{w,i}$	Molar weight of component I [kg mol^{-1}]
N_i	Molar flux component i [mol m^{-2} s^{-1}]
p_0	Pre-exponential factor for permeability of membrane [mol m^{-1} s^{-1} Pa^{-n}]
P_i	Partial pressure of species i [bar]
r_j	Reaction rate of reaction j [mol kg^{-1} s^{-1}]
$R_{memb.}$	Radius of the membrane
$SF(Q)$	Heaviside function of Q
t	Thickness of Membrane selective layer thickness [m]
$u_{k,n}^s$	Superficial velocity of phase j in cell k [m s^{-1}]
u_{mf}	Minimum fluidization velocity [m s^{-1}]
u_0	Superficial gas velocity at inlet
u_b	Bubble rise velocity
$u_{b,avg}$	Average bubble rise velocity
$V_{D,i}$	Diffusion volume for component i
$V_{k,n}$	Volume of phase k in cell n [m^3]
$w_{k,i,n}$	Weight fraction of phase k, component i in cell n
$x_{i,bulk}$	Molar fraction of species i in the bulk
$x_{i,memb.}$	Molar fraction of species i adjacent to the membrane

Greek symbols

δ	Thickness of the stagnant film layer [m]
ΔH_r^θ	Reaction enthalpy at standard conditions [kJ/mol]
$\varepsilon_{k,n}$	Fraction of phase k in cell n
ε_{mf}	Bed voidage at minimum fluidization velocity
μ_g	Gas viscosity [Pa s]
$\nu_{j,i}$	Stoichiometric coefficient of reaction j component i
$\rho_{k,n}$	Density of phase k in cell n [kg m^{-3}]

Subscripts

b	Bubble phase
e	Emulsion phase
g	Gas phase
i	Species
j	Reaction
n	Number of CSTR in emulsion or bubble phase
s	Solid phase

temperatures over a nickel-based catalyst to produce CO and H$_2$ via the Steam Methane Reforming reaction (SMR), Eq. (1). To increase the hydrogen yield this process is combined with Water Gas Shift (WGS), Eq. (2). Because of the high CO$_2$ content, Dry Reforming (DR), Eq. (3), is likely to take place as well.

$$CH_4 + H_2O \rightleftarrows CO + 3H_2 \quad \Delta H_r^\theta = +206\,\mathrm{kJ\,mol^{-1}} \tag{1}$$

$$CO + H_2O \rightleftarrows CO_2 + H_2 \quad \Delta H_r^\theta = -41\,\mathrm{kJ\,mol^{-1}} \tag{2}$$

$$CH_4 + CO_2 \rightleftarrows 2CO + 2H_2 \quad \Delta H_r^\theta = +247\,\mathrm{kJ\,mol^{-1}} \tag{3}$$

The reforming of methane is highly endothermic and requires high temperatures (> 900 °C) and is favoured at low pressures. Moreover, to obtain high purity hydrogen from the SR process, downstream separation and purification steps are required. The application of biogas in the SR process has significant challenges: (i) the combination of the nickel catalyst and high operation temperatures makes the system prone to

Table 1
Anaerobic digestion or landfill biogas composition [2].

Component	AD biogas	Landfill biogas	Unit
CH$_4$	53–70	30–65	vol%
CO$_2$	30–50	25–47	vol%
N$_2$	2–6	< 1–17	vol%
O$_2$	0–5	< 1–3	vol%
H$_2$	NA	0–3	vol%
C$_x$H$_y$	NA	NA	vol%
H$_2$S	0–2000	30–500	ppm
NH$_3$	< 100	0–5	ppm
Chlorines	< 0.25	0.3–225	mg Nm^3
Siloxane	< 0.08–0.5		μg/g-dry

coking, (ii) the high CO$_2$ content of biogas induces equilibrium limitations and (iii) the presence of H$_2$S even if present in trace amounts requires intensive cleaning of the biogas. The development of reforming catalysts with a high resistancy to carbon formation have increased the potential for hydrogen production from biogas [3]. Noble metal catalysts, such as Rh, Ru, Pt and Pd show a high activity and selectivity for hydrogen production [4]. Generally Rh has been found to have the best performance along the different noble metal catalysts. To remove the H$_2$S, the biogas can be upgraded by cleaning using e.g. pressurized water scrubbing, pressure swing adsorption, amine absorption or membrane absorption [2]. However, these methods significantly increase the energy consumption and costs of hydrogen [2]. The emerging technology of palladium-based membrane reactors shows a high degree of process intensification for the production of hydrogen and has demonstrated significant advantages over the conventional SR process [5]. The hydrogen is selectively extracted from the reaction system, thus combining the SMR, WGS and H$_2$ separation (and purification) in one single unit. The in-situ extraction of hydrogen can overcome the equilibrium limitations of the biogas reforming thanks to the product recovery. The shift in equilibrium also allows operation at lower temperatures and higher pressures. Finally, pure hydrogen is obtained directly from the membranes without the requirement of downstream separations, hence reducing the process complexity and the associated capital costs. These advantages of membrane reactors can make hydrogen production on smaller scales from a decentralized source such as biogas attractive. Previous works investigated the application of biogas steam reforming in a membrane reactor. Sato et al. [6] identified the membrane reactor as a promising technology for hydrogen production from biogas. Steam reforming of a biogas mixture derived from supercritical water gasification of glucose was performed using a PdAg

supported on stainless steel membrane in a fixed bed containing a Ru/Al₂O₃ catalyst. Iulianelli et al. [7] studied the steam reforming of biogas in a Pd-based membrane on a porous Al₂O₃ support over a Ni catalyst. Methane conversion of 34% and separation of the produced hydrogen up to 70% were reported. However, the process required regeneration of the catalyst deactivated by carbon formation, and the hydrogen purity was decreased rapidly due to the formation of pinholes. Vasquez et al. [8] investigated the effect of the temperature and pressure on the steam reforming in a fixed bed and described their experiments with a one-dimensional model. However, the use of fixed-bed reactors has some drawbacks, in particular when applied to membrane reactors with high fluxes. First of all, the poor heat transfer in the packed bed results in large temperature gradients, which can be detrimental for the membrane flux and membrane stability. Moreover, when high-flux membranes are used, mass transfer limitations, known as concentration polarisation, become dominant and negatively impact the reactor performance [9,10]. The mass transfer limitations depend on the hydrogen depletion close the membrane surface and prevails when the hydrogen transport from the bulk in the fixed bed to the membrane surface is relatively slow. As a result, concentration polarisation decreases the trans-membrane driving force for the hydrogen transport. These aspects can be reduced by using fluidized bed membrane reactors, which have significantly higher heat transfer rates compared to fixed bed membrane reactors, resulting in advantages in terms of heat management and a much more even temperature distribution [11]. Moreover, it is expected that the higher mass transfer rates also result in a reduction of the concentration polarisation.

However, when describing the steam reforming of biogas in a fluidized bed membrane reactor, the concentration polarisation is still expected to influence the system performance significantly. These effects are a result of the low methane and consequently hydrogen concentrations and cannot be ignored. The present work evaluates a fluidized bed membrane reactor for biogas steam reforming and the influence of concentration polarisation on the system performance. The effect of concentration polarisation is first analysed experimentally for hydrogen/nitrogen mixtures with and without the fluidized bed. The steam reforming of synthetic biogas mixtures (mainly CO₂ and CH₄) as well as pure methane is evaluated for temperatures between 430 °C and 530 °C and pressures up to 5 bar. The results are discussed, followed by the description and validation of a developed phenomenological, one-dimensional, two-phase fluidized bed membrane reactor model. The model is then used to quantify the influence of the concentration polarisation and its significance for the design of fluidized bed membrane reactors for biogas reforming.

2. Experimental

2.1. Experimental setup

Single and mixed gas permeation tests to characterize the membrane performance and reforming experiments, were conducted in a membrane reactor consisting of a shell-and-tube configuration (see Fig. 1) where the reactor has a diameter of 4.27 cm and a total length of 44 cm. The membrane is made of a thin PdAg layer deposited by electroless plating onto an alumina porous tube from Rauschert. The membrane was sealed using a graphite sealing method developed by Fernandez et al. and the leakage was subsequently measured using an helium/ethanol system [12]. The length of the membrane was 14.35 cm and with a diameter of 14.26 mm resulting in a total membrane surface area of 64.3 cm². The membrane thickness was measured by SEM (Phenom) analysis on a cross section of the membrane and was found to be 5.2 μm. The membrane was integrated from the top flange of the reactor with a stainless-steel tube, such that a distance of 2 cm remained between the bottom gas distributor and the bottom membrane seal. Single and mix gas experiments were performed first without catalyst particles, here referred to as empty tube. After these experiments the catalyst, a Rh based catalyst supplied by Johnson Matthey (particle size of 170 μm), was loaded into the reactor to perform the mix gas test under fluidized conditions and subsequently the (steam) reforming experiments. The reactor system could be operated in two configurations, viz. as a normal fluidized bed reformer and as a fluidized bed membrane reactor, simply by opening and closing of the membrane permeate line. The minimum fluidization velocity of the catalyst was experimentally determined at different temperatures and atmospheric pressure using the standard pressure-drop method. The feed flow rate for reactive experiments was selected in such a way that the fluidized bed was in the bubbling fluidization regime. The amount of catalyst was selected to cover the full active membrane surface, resulting in 165 g of catalyst. The reactor was placed inside an oven to ensure isothermal operation. In the reforming experiments the temperature, pressure and feed gas composition was varied. The system performance was evaluated in terms of methane conversion (Eq. (4)), separation factor (SF, Eq. (5)) and hydrogen recovery factor (HRF, Eq. (6)) as defined below:

$$Methane\ conversion = \frac{(F_{CH_4,in} - F_{CH_4,out})}{F_{CH_4,in}} \tag{4}$$

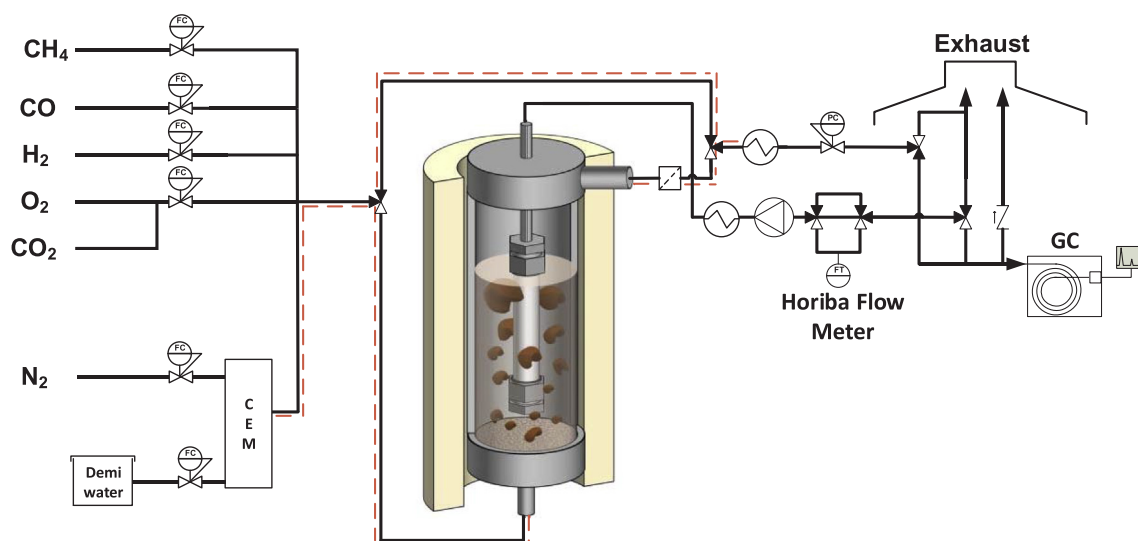**Fig. 1.** Schematic representation of the experimental setup.

$$Separation\,factor = \frac{F_{H_2,perm}}{(F_{H_2,perm} + F_{H_2,ret.})} \tag{5}$$

$$Hydrogen\,recovery\,factor = \frac{F_{H_2,perm}}{4F_{CH_4,in}} \tag{6}$$

The gas feed to the reactor was controlled by Bronkhorst® digital mass flow controllers. The feed of water was controlled by a Bronkhorst® Coriflow liquid meter and steam was produced using a Bronkhorst® controlled evaporator mixer. The pressure was controlled by a back pressure regulator supplied by Bronkhorst®. The permeate side was either operated at atmospheric pressure or at vacuum. The volumetric flow rate at the permeate side was measured using a Horiba film flow meter. The composition of both the permeate and retentate streams were measured using a Varian micro GC equipped with two molecular sieve 5A columns and a PoraPlot Q column. The retentate flow rate is obtained from the nitrogen balance. The carbon balance was satisfied with ± 5% error for all experiments reported hereafter. The system has been tested at CH₄/H₂O ratios high enough such that carbon formation is thermodynamically unlikely to occur. The membrane has been visually inspected after the test and no carbon formation was found. The catalyst has been analysed using thermogravimetric analyses and no carbon formation was found.

2.2. Membrane performance characterization

Once the membrane was placed in the reactor, the nitrogen leakage was monitored periodically. To activate the membrane, the system was heated up to 400 °C in nitrogen, once at this temperature the membrane was exposed to 2 Nl/min of air for 2 min. Subsequently, the system was flushed with nitrogen and heated up to 550 °C and left in a hydrogen environment until a stable hydrogen flux was obtained. After reaching stable conditions, the permeation tests were performed decreasing the oven temperature from 550 °C to 400 °C with steps of 50 °C; the results are shown in Fig. 2. The hydrogen permeability of the membrane could be well described as a function of the driving force using an exponent n equal to 0.5 (i.e. Sieverts' law), as shown in Fig. 2. An activation energy and a pre-exponential factor of respectively 9.23 kJ/mol and $4.57 \cdot 10^{-8}\,mol\,m^{-1}\,s^{-1}\,Pa^{-0.5}$ were fitted to the experimental data. These values are comparable with the 9.99 kJ/mol and $6.93 \cdot 10^{-8}\,mol\,m^{-1}\,s^{-1}\,Pa^{-0.5}$ reported earlier by Fernandez et al. for a similar membrane [13]. The initial ideal H₂/N₂ perm-selectivity was found to be 18,000 at 545 °C and 4576 at 384 °C with a transmembrane pressure difference of 1 bar.

3. Model description

The reactor model developed in this work describes a membrane fluidized bed section in which a dead-end perm-selective membrane can be integrated. It is an improvement of the model described by Gallucci et al. [14]. The model was firstly developed by Deshmukh et al. and based on the frequently used bubble assemblage model proposed by Kato and Wen [15,16]. In this approach, both the bubble and emulsion phases are divided into a number of CSTRs along the reactor. In particular, Kato and Wen related the volume of the CSTR to the local bubble size, whereas Deshmukh et al. adopted a different approach where the CSTRs all have the same volume and the number of CSTRs is used describe the amount of gas back mixing in the system [15,17].

The steady state overall (bubble and emulsion phases) component mass conservation equations, the total volume balance and the overall balances for each component used in the model are formulated in Table 2. These equations consider the chemical transformations in the emulsion phase and a net gas production due to the chemical reactions and gas extraction via the membrane. The equations are solved for each section in the fluidized bed reactor. Since the introduction of membrane reduces the extent of back mixing, a large number of CSTRs is selected

representing plug flow behaviour. The empirical correlations for the description of the system hydrodynamics and mass transfer are obtained from literature and are described in Appendix I [16,18–20]. Although these equations are developed for fluidized beds without membranes, it is shown in prior works that a reasonable description of the system with immersed membranes can also be obtained [14,17]. The chemical reactions are described using the kinetic rate laws by Numaguchi and Kikuchi for the steam reforming and water gas shift reactions [21]. The kinetic parameters for the Rh based catalyst are obtained from Marra et al. [22]. The rate expressions and kinetic parameters are provided in Appendix II. Because of the high steam-to-carbon ratio applied in the experimental conditions the dry reforming reaction can be assumed to be of negligible influence in the reaction system (this was also confirmed by separate kinetic tests not reported here for brevity).

The selective extraction of hydrogen in the model is described by Sieverts' law, Eq. (7), using the experimentally obtained parameters of the membrane.

$$N_i = \frac{p_0}{t}e^{Ea/RT}(P^n_{H_2,Ret.} - P^n_{H_2,Perm.}) \tag{7}$$

When describing hydrogen extraction from a mixture through a highly selective and permeable membrane, Sieverts' law is found to be insufficient to predict the transmembrane flux [24,25]. Due to the depletion of the permeable species near the membrane and accumulation of the non-permeable species, a mass transfer boundary layer is formed along the membrane (phenomena known as concentration polarisation). To account for the mass transfer limitations induced and accurately describe the membrane permeation, the concentration at the membrane surface is required. In this work, the stagnant film model is applied to determine the concentration at the membrane surface [26]. In the stagnant film model, the following assumptions are applied:

- Steady state conditions;
- No axial convection in the film layer;
- No axial dispersion, only radial dispersion.
- The thickness of the stagnant film is assumed to remain constant along the length of the membrane.

The boundary layer thickness is indicated with δ, see Fig. 3. The steady state mass balance of the shell around a cylindrical membrane in the radial direction, as shown in Fig. 3, leads to Eq. (8), where $N_{i,r}$ is the flux in the radial direction.
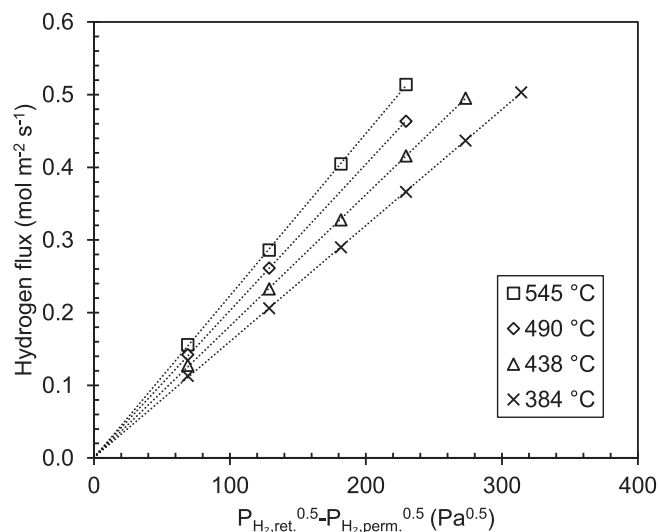

Fig. 2. Single gas test permeation results of hydrogen.

Table 2

Mass balance equations for each CSTR in each section of the fluidized bed membrane reactor [23].

Total mass balance

$$u_{b,n-1}^s A_T \rho_{b,n-1} - u_{b,n}^s A_T \rho_{b,n} + u_{e,n-1}^s A_T \rho_{e,n-1} - u_{e,n}^s A_T \rho_{e,n}$$

$$+ \sum_{i=1}^{nc} (N_{i,mol}^{membrane} M_{w,i} A_{membrane} \varepsilon_{b,n} + N_{i,mol}^{membrane} M_{w,i} A_{membrane} (1-\varepsilon_{b,n})) = 0$$

Bubble phase component mass balance

$$u_{b,n-1}^s A_T \rho_{b,n-1} - u_{b,n}^s A_T \rho_{b,n} - \sum_{i=1}^{nc} K_{be,i,n} V_{b,n} \rho_{b,n} (w_{b,i,n} - w_{e,i,n})$$

$$+ \sum_{i=1}^{nc} N_{i,mol}^{membrane} M_{w,i} A_{membrane} \varepsilon_{b,n} + [w_{e,i,n} SF(Q) - w_{b,i,n} SF(-Q)] = 0$$

Emulsion phase component mass balance

$$u_{e,n-1}^s A_T \rho_{e,n-1} - u_{e,n}^s A_T \rho_{e,n} + \sum_{i=1}^{nc} K_{be,i,n} V_{b,n} \rho_{b,n} (w_{b,i,n} - w_{e,i,n})$$

$$+ \sum_{i=1}^{nc} N_{i,mol}^{membrane} M_{w,i} A_{membrane} (1-\varepsilon_{b,n}) - \left(\sum_{j=1}^{nrxn} \nu_{j,i} r_j \right) V_{e,n} \rho_{p,n} (1-\varepsilon_e)$$

$$+ [w_{e,i,n} SF(Q) - w_{b,i,n} SF(-Q)] = 0$$

Transfer term

$$Q = u_{e,n-1}^s A_T \rho_{e,n-1} - u_{e,n}^s A_T \rho_{e,n} + \sum_{i=1}^{nc} K_{be,i,n} V_{b,n} \rho_{b,n} (w_{b,i,n} - w_{e,i,n})$$

$$\pm \sum_{i=1}^{nc} N_{i,mol}^{membrane} M_{w,i} A_{membrane} (1-\varepsilon_{b,n})$$

$$u_{e,n}^s A_T = u_{e,n} A_T (1-\varepsilon_{b,n})$$

$$u_{b,0}^s A_T = u_{tot} A_T \varepsilon_{b,n}$$

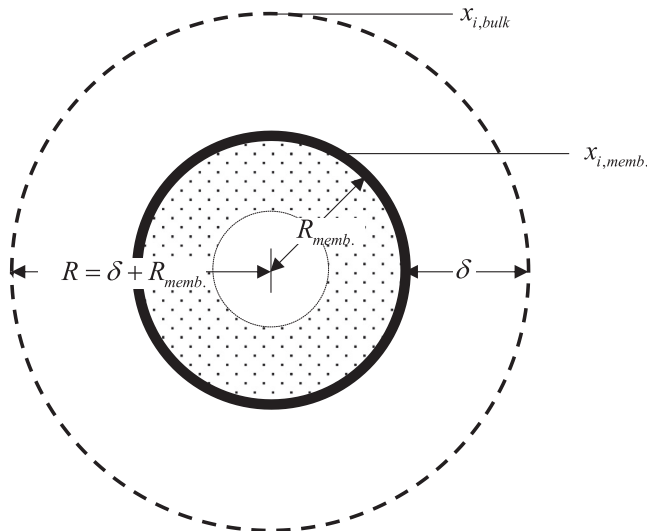$$u_{b,0}^s A_T = u_{tot} A_T (1-\varepsilon_{b,n})$$

Fig. 3. Schematic description of the film around the membrane.

$$-\frac{1}{r}\frac{d}{dr}(r N_{i,r}) = 0 \tag{8}$$

The total flux through the film layer in the radial direction can be written as the sum of the drift flux and diffusive mass flux, Eq. (9), using the generalised Fick's law, where D_i represents the effective diffusivity of component i and C_{tot} the total concentration.

$$N_{i,r} = -D_i C_{tot} \frac{dx_i}{dr} + x_i N_{tot} \tag{9}$$

Since the membrane can be approximated as fully permselective for H_2, N_{tot} equals $N_{i,r}$, so further rearranging Eq. (9) leads to Eq. (10).

$$N_{i,r} = -D_i C_{tot} \frac{1}{1-x_i} \frac{dx_i}{dr} \tag{10}$$

From the steady state mass balance, it follows that the term $r N_{i,r}$ is constant over the layer.

$$r N_{i,r} = c \text{ at } r = R_{memb.} + \delta, N_{i,r} = N_{i,r_m+\delta} \tag{11}$$

Combining this and Eq. (10) and integrating over the boundary layer of thickness δ yields Eq. (12)
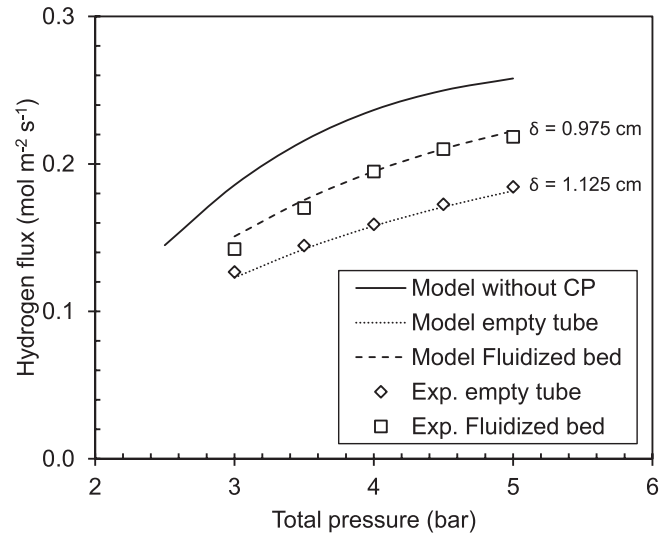

Fig. 4. Permeated hydrogen flux at different total pressures from a 75% H_2/N_2 mixture at 380 °C, with a total feed flow of 3.6 Nl/min.

$$N_{i,r_m+\delta} = \frac{D_i C_{tot}}{R_{memb.} + \delta \ln\left(1 + \frac{\delta}{R_{memb.}}\right)} \ln\left(\frac{1-x_{i,memb.}}{1-x_{i,bulk}}\right) \tag{12}$$

Since the flux through film layer and membrane are equal, Eq. (12) can be used to find $x_{i,memb.}$ and obtain the partial pressure of hydrogen at the surface of the membrane.

4. Results and discussion

4.1. Permeation of N_2 and H_2 mixtures

Gas permeation experiments were performed to determine the influence of the concentration polarisation on the membrane separation and to validate the implementation of the stagnant film in the model. Hydrogen permeation in the empty tube system (no catalyst bed) from a 75% H_2/N_2 mixture was measured at different pressures. After these experiments the catalyst was loaded into the system. The presence of the catalyst should not influence the hydrogen permeation from a pure hydrogen mixture. However, the experiment with the 75% H_2/N_2 mixture showed that the flux was increased compared to the empty tube system. In Fig. 4, the experimental results are shown together with the model results.

The extent of the concentration polarisation can be represented by the Concentration Polarisation Coefficient (CPC). Several definitions of the CPC exist in literature however in this work the definition presented by Caravella et al. is used [24]. Taking the logarithmic average into account in determining the pressure difference over the module. The CPC for both the results of the empty and fluidized bed system permeation test are shown in Fig. 5. The concentration polarisation coefficient is reduced by the introduction of the fluidized bed from 0.41 to 0.32 at 3 bar, at 5 bar is decreased from 0.52 to 0.34.

Because the model without concentration polarisation does not take mass transfer limitations into account, the hydrogen flux is over-predicted. This shows that a description taking the concentration polarisation into account is indeed required in the model. To describe the permeation results in the empty tube system, a δ of 1.125 cm was fitted to the experiment at 4 bar total pressure. In the work of Helmi et al. [27] it is shown that the radial dispersion in the fluidized bed is larger than the molecular gas diffusion coefficient D_i. Since there is no general correlation available for the radial dispersion in membrane fluidized beds its value was estimated using CFD simulations at $1 \cdot 10^{-4}$, which was also adopted in this work. Accordingly, a δ of 0.975 cm was found to correctly describe the hydrogen flux. The increase in the hydrogen
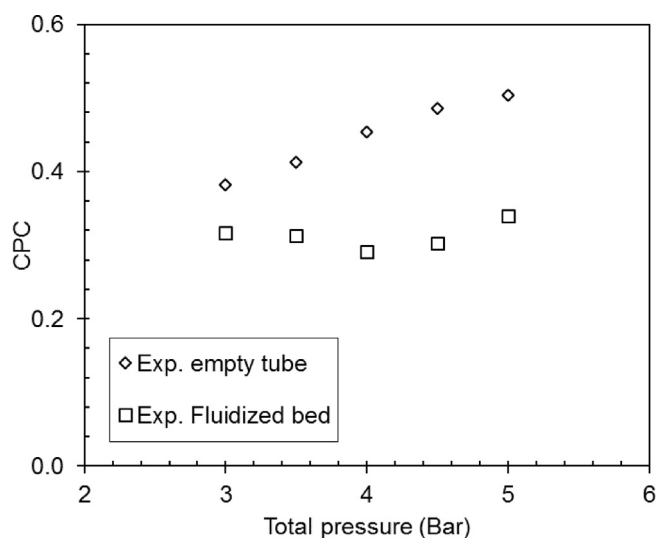
Fig. 5. Concentration polarisation coefficient for the empty tube and the fluidized bed system at different pressures.

flux in the fluidized bed compared to the empty system can thus be explained by the increase of the radial dispersion of the system due to the bubbling behaviour of the fluidized bed corresponding to a decrease in δ.

Fig. 5a shows the film layer thickness at 3 bar fitted for different feed fractions of hydrogen in the system without fluidized bed for different total feed flow rates. To indicate the effect of hydrogen depletion on the results, the bars in Fig. 5 show the inlet and outlet fraction of hydrogen of the system. The film layer thickness increases with an increase in the partial pressure of hydrogen, roughly between 6 and 12 mm. Analysis of the conditions of these results show that the decrease in δ with a decrease of the partial pressure of hydrogen and fluidization velocity is related to the increase in the Reynolds number of the system, as shown in Fig. 5b, demonstrating the strong influence of the hydrodynamics on the extent of the concentration polarisation. However, for the fluidized bed there is no correlation available to get a good estimation of the δ as a function of the different operating conditions. Therefore, in this work δ is an adjustable parameter of the model and obtained by fitting to the results of a base case reforming

experiment performed at the following conditions: 480 °C, a total pressure of 3 bar, a total feed flow rate of 3.6 Nl/min and a feed distribution of $CH_4:CO_2:H_2O = 1:0.7:3$. The δ obtained from the fitting was 0.54 cm as a result of the more vigorous hydrodynamics of the fluidized bed; this constant δ is further used to describe all reforming experiments presented in the following analysis. The CPC for the system with biogas reforming was found to be 0.78, with the use of the hydrogen concentrations obtained from the model.

4.2. Biogas steam reforming

To validate the model for the reforming of synthetic biogas, experiments were carried out at temperatures between 430 °C and 540 °C, with CO_2/CH_4 feed ratios ranging from 0 to 0.9, pressures from 2 bar up to 5 bar and a range of steam-to-carbon ratios (SCR) from 2 to 4. The stability of the system was monitored using the prior mentioned base case experiment together with the performance of the membrane. The nitrogen and hydrogen permeability of the membrane increased over time: the fluidization roughens the membrane surface increasing the active area for hydrogen permeation but also creating defects for nitrogen to pass. The discrepancy between the model and experiments was therefore higher for the experiments varying the SCR, as they were performed in a later stage of the system. All other results showed good agreement with the model and the use of one single δ showed to be sufficient over the investigated experimental ranges. From Figs. 6 to 9 the experimental results together with the model predictions are shown in terms of methane conversion, SF and HRF. The effects of the studied parameters will be further elaborated to show the effects and the differences between methane steam reforming (MSR) and biogas steam reforming (BSR). The impact of the temperature is studied for three different values, a comparison is made between MSR and BSR, all the other parameters are studied with and without the selective extraction of hydrogen. In all cases, the experimental results and the model prediction fit with the predicted equilibrium conversion. The cases without extraction of hydrogen behaved as expected for SMR: the methane conversion increases with temperature due to the endothermic nature of the system (Fig. 6); a decrease in methane conversion with increasing pressure as a result of the negative effect of pressure on the SMR reaction (Fig. 7) and when CO_2 in the feed is increased, to form the synthetic biogas mixture, the conversion reduces due to the high concentration of CO_2 (Figs. 6 and 8). The increase in H_2O content on the other hand had a positive effect on the methane conversion, since this is
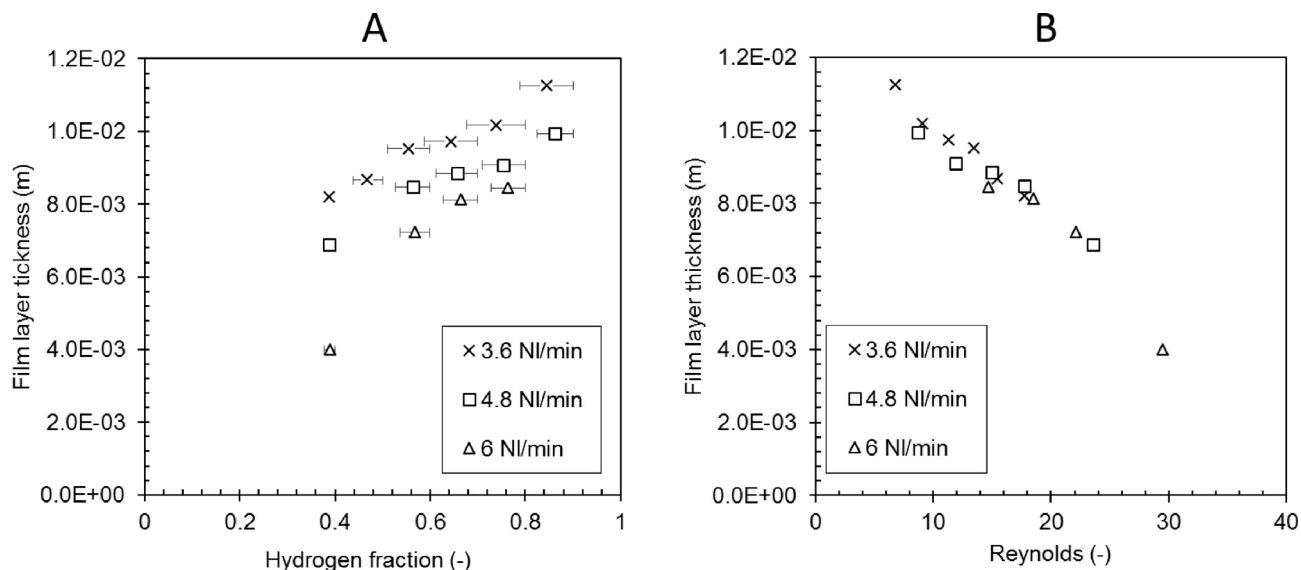

Fig. 6. A: Film layer thickness for different hydrogen fractions at 3 bar and 370 °C for different total feed flow rates in system without fluidized bed. B: the thickness of the boundary layer as function of the Reynolds number.
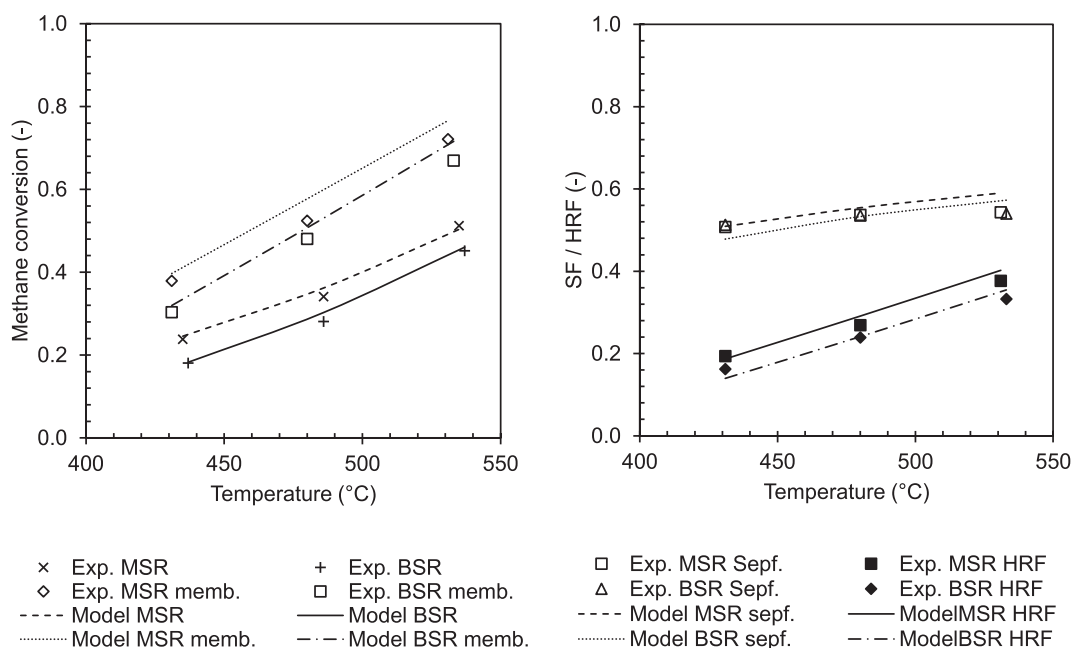
Fig. 7. Methane conversion, SF and HRF of SMR and BSR (CO_2/CH_4 = 0.7) as a function of temperature at 3 bar, a total feed of 3.6 Nl/min with 10% of methane and a SCR of 3.

a reactant forcing the equilibrium to the product side (Fig. 9). When hydrogen was extracted from the system the equilibrium was shifted upwards. The extent of this shift depends on the permeability of the membrane and the transmembrane driving force. Focusing on temperature, the permeability of the membrane increases with temperature showing a higher SF and HRF and thus shift of the conversion. A maximum methane conversion of 72% and 68% for respectively MSR and BSR at 533 °C was obtained. The transmembrane pressure is strictly related to the system pressure, therefore increasing the pressure results in an increase of SF as well as HRF. Over the tested range, the conversion increased by 50% to 105% with respect to the conversion without membrane. Although, it was not possible to work at higher pressures in the experimental system it can be expected that at higher pressure, hence higher HRF, the conversion would increase with pressure. In this way, the system can overcome the negative effect of the pressure on the SMR reaction. The study of different BSR mixtures with different CO_2/CH_4 ratios showed a constant shift in equilibrium, as the SF was not affected by the higher feed of CO_2. The equilibrium

conversion and HRF still decreased with an increase in the CO_2 fraction and also the concentration of CO was increased on the retentate side with increasing CO_2/CH_4, showing the effect of the CO_2 on the WGS equilibrium. CO poisoning could be assumed to be negligible, as the SF was not affected and considering the temperature the experiments where performed at [28]. The dilution effect of CO_2 could not be studied well in these experiments since the system feed was balanced with CO_2, later performed experiments with lower dilutions also showed no significant effect of an increase in the CO_2 content in the feed on the SF. As mentioned before, the methane conversion increases with higher SCR, however, also the shift showed a small increase. This increase in shift can be explained as follows: as more hydrogen is produced, also the transmembrane pressure difference is increased, which can be seen from a slight increase in SF. During the experiments, there was no indication of carbon formation, and after the experiment no carbon was visible in the system or on the membrane.

The methane conversion, SF and HRF are important parameters to assess the reactor performance, although the purity of the hydrogen is
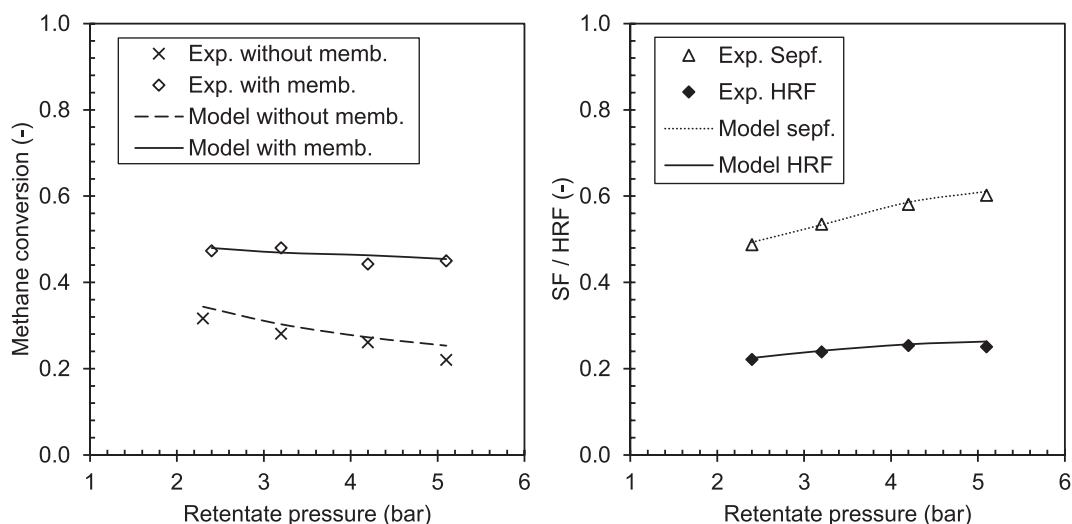

Fig. 8. Methane conversion, SF and HRF for different pressures at 480 °C, a total feed of 3.6 Nl/min with 10% of methane and a SCR of 3.
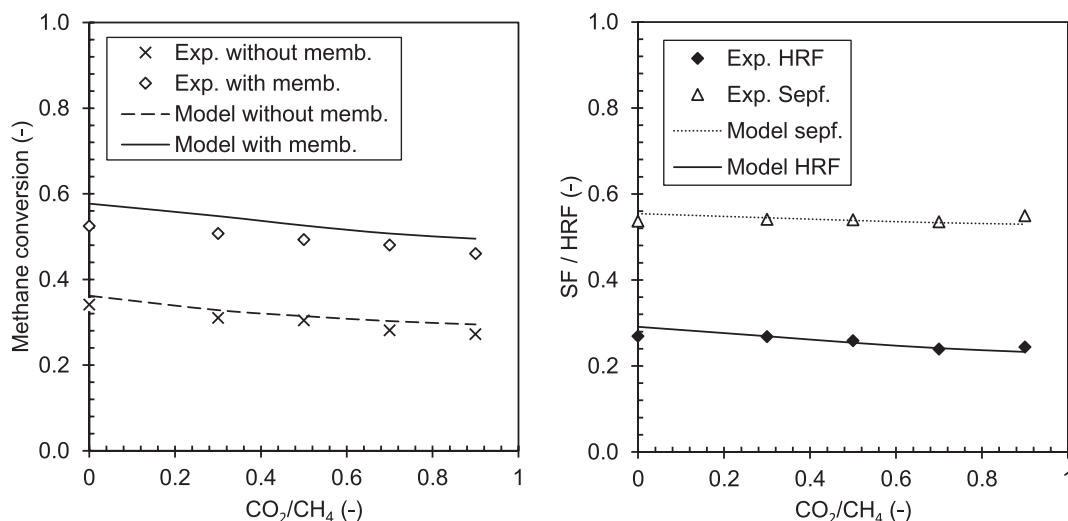
Fig. 9. Methane conversion, SF and HRF for different CO_2/CH_4 ratios at 480 °C, 3 bar, a total feed of 3.6 Nl/min with 10% of methane and a SCR of 3.

as important to demonstrate the potential of the presented concept for biogas steam reforming. The permeate composition for the different cases is reported in Fig. 10. The minimum amount of CO that was detected at the permeate side in the experiments was 146 ppm, in the other cases the GC was not detecting any CO and the amount can be assumed to be at least lower than 146 ppm. CO was found in three cases, where in two of the cases the CO concentration in the system was relatively high as a result of the high CO_2/CH_4 ratio or the low SCR, while in the other case the temperature was lower (437 °C) resulting in a lower hydrogen flux. The hydrogen purity is strongly affected by the temperature, because it affects the hydrogen flux as consequence of the increased the hydrogen permeability and methane conversion at higher temperatures. The lowest and highest hydrogen purity found for BSR were 97.34% and 99.88% achieved at the lowest and highest operation temperature, respectively. This effect could also already be seen from the increase in the ideal selectivity during the membrane characterization.

4.3. Optimization and scale-up

To further validate the implementation of the concentration polarisation in the model, experiments with high dilutions were performed. From the results of these experiments a higher discrepancy with the model for the flux was obtained. This can be discerned from Fig. 11, where the high and the low dilution cases are compared. This discrepancy can be explained by the increase in the hydrogen partial pressure in the system and the change in validity of the assumed film layer thickness.

Further scale up of the system to higher pressures would therefore require a new estimation of δ. However, no Sherwood correlation is available in the literature to describe the mass transfer from the bulk to the immersed membrane. To study the importance of the parameter δ, the validated model is used to evaluate this. To do this, the model was scaled up and the operation conditions were selected as for an industrial application. The system feed was selected as a representative biogas reforming mixture. Both the feed composition and the operation conditions are listed in Table 3 and the computed concentration profile along the reactor length is shown in Fig. 12.

It can be seen, that in the first part most of the hydrogen is produced and the highest hydrogen concentration is reached. After this point the rate of hydrogen extraction becomes dominant over the rate of hydrogen production, and therefore the hydrogen concentration decreases along the reactor. Both the steam and methane concentration decrease along the reactor as they are converted. CO_2 is produced together with CO. A small difference can be outlined between the emulsion phase and bubble phase concentrations due to the influence of bubble-to-emulsion phase mass transfer limitations. This is not the case for the hydrogen transport, since in the model it was assumed that hydrogen is extracted
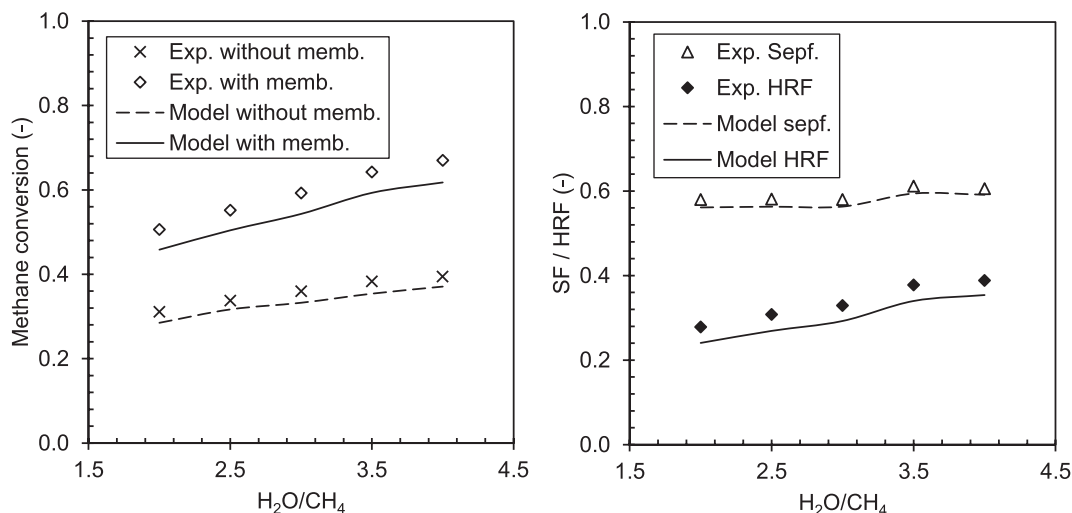

Fig. 10. Methane conversion, SF and HRF for different SCRs at 480 °C, 3 bar and a total feed of 3.6 Nl/min with 10% of methane.
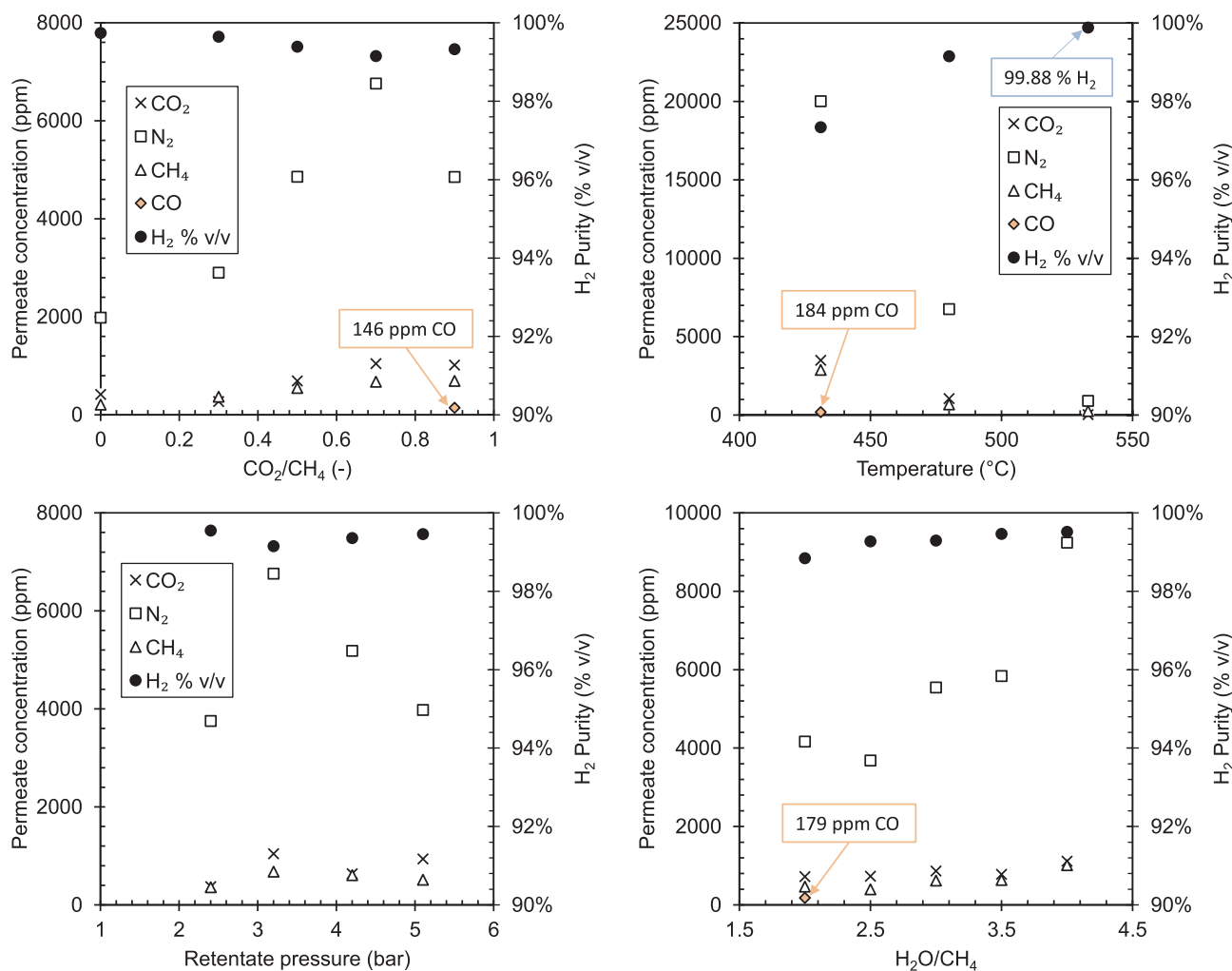
Fig. 11. Permeate composition for: (a) CO_2/CH_4 ratio, (b) temperature, (c) pressure and (d) SCR.

Table 3
Conditions and feed composition used for the analyses of the scaled-up system.

Parameter	value	Unit
Pressure	12	bar
Temperature	550	°C
Permeate pressure	0.1	bar
H_2O/CH_4	2.4	–
CO_2/CH_4	0.76	–
N_2/CH_4	0.37	–
u/u_{mf}	7.41	–

Fig. 12. Parity plot of the predicted and measured hydrogen flow for high and low dilution conditions.

from both the emulsion and bubble phase. To evaluate the importance of the thickness δ, the system was evaluated for three different cases: δ equal to 0.54 cm as resulted from the permeation experiments, a δ of 0.25 cm and 0.75 cm. The results of these calculations are shown in Fig. 13. The thickness δ has a significant influence on the system performance. The conversion is shown as function of the membrane productivity, indicating the amount of hydrogen that can be obtained per membrane area. The productivity of the membranes reduces proportionally with the thickness of δ. Which means that a decrease in thickness δ of 25% leads in an increase of 25% in the productivity. These results not only highlight the importance of the film layer thickness in the design of fluidized bed membrane reactors, but also indicate the potential of improving a membrane system by decreasing the concentration polarisation (See Fig 14).
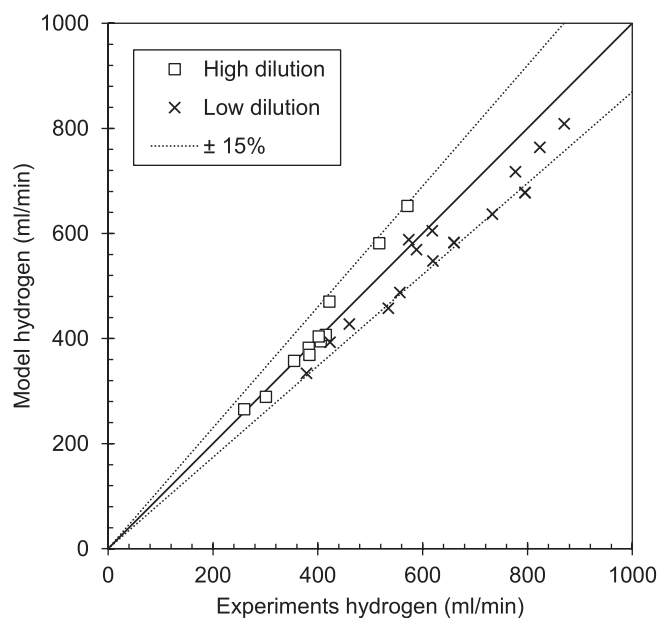
Fig. 13. Composition along the reactor at 550 °C, 12 bar, load-to-surface ratio of $3 \, m^3_{CH_4\text{-memb.}} \, h^{-1}$, continues lines and dashed lines represent respectively emulsion and bubble phase gas fractions.

Fig. 14. Membrane productivity as function of methane conversion for three different thicknesses of δ.

5. Conclusions

Hydrogen production via steam reforming of biogas has been experimentally investigated in a fluidized bed membrane reactor and the results were used to validate a phenomenological, one-dimensional, two-phase model, that was extended to account for concentration polarisation using a stagnant boundary layer film model. A PdAg membrane supported on Al_2O_3 has been used both in an empty shell-and-tube configuration and in a fluidized bed with a Jonson Matthey Rh based catalyst. Permeation results in the various system configurations were used to determine the thickness of the mass transfer boundary layer (δ). The importance of the hydrogen concentration and fluidization velocity on the extent of concentration polarisation is shown. A good description of the reforming experiments over the entire range of experimental conditions was obtained by the model when using the same thickness δ of 0.54 cm. Experiments with synthetic biogas mixtures showed lower conversions, however, the hydrogen separation was not affected and the previous estimation of δ was sufficient. However, when scaling up the system to lower dilutions showed a larger error in the model predictions. The model was used to further scale up the system and study the dependency of the thickness δ. It was shown that the thickness significantly influenced the system productivity and δ scaled proportionally with the productivity.

Appendix

Appendix I. Empirical correlation used in the model for the description of the system hydrodynamics and mass transfer

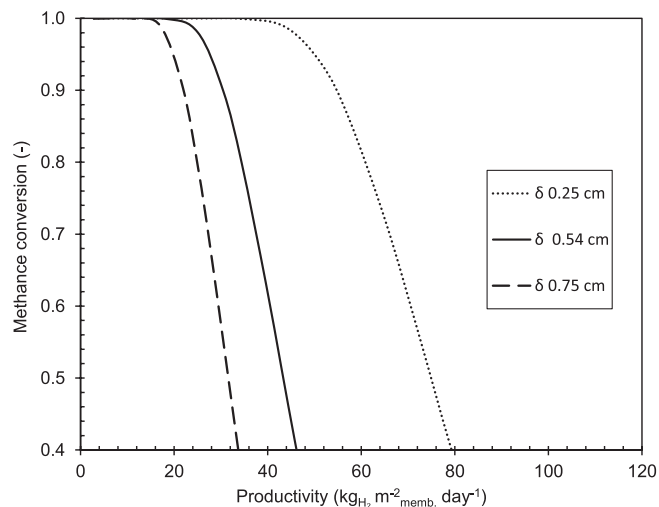| Parameter	Equation	Refs.
Archimedes number	$Ar = \dfrac{d_p^3 \rho_g (\rho_p - \rho_g)}{\mu_g^2} g$	
Minimum fluidization velocity	$u_{mf} = \left(\dfrac{\mu_g}{\rho_g d_p}\right)\left(\sqrt{(27.2)^2 + 0.0408 Ar} - 27.2\right)$	[19]
Bed voidage at minimum fluidization velocity	$\varepsilon_{mf} = 0.586 Ar^{-0.29}\left(\dfrac{\rho_g}{\rho_p}\right)^{0.021}$	[19]
Projected reactor area	$A_T = \dfrac{\pi}{4} D_T^2$	
Bubble diameter	$d_b = d_{b,\max} - (d_{b,\max} - d_{b,0}) e^{\left(\frac{0.3z}{D_T}\right)}$	[18]
Initial bubble diameter	$d_{b,0} = 0.376 (u_0 - u_{mf})^2$	[20]
Maximum bubble diameter	$d_{b,\max} = \min(1.6374 A_T (u_0 - u_{mf}); D_T)$	
Average bubble diameter	$d_{b,avg} = \dfrac{d_{b,\max} + (d_{b,\max} - d_{b,0})\frac{D_T}{0.3}}{H_2 - H_1}\left(e^{-0.3\frac{H_2}{D_T}} - e^{-0.3\frac{H_1}{D_T}}\right)$	
Average bubble rise	$u_{b,avg} = u_0 - u_{mf} + 0.711 (g d_{b,avg})^{0.5}$	
Emulsion velocity	$u_e = \dfrac{u_0 - f_b u_b}{1 - f_b}$	

Bubble phase fraction	$f_b = \frac{u_0 - u_{mf}}{u_{b,avg}}$	[16]
Emulsion phase fraction	$f_e = 1 - f_b$	
Initial superficial bubble gas velocity	$u_{b,0}^s = u_{b,0} f_{b,o} \quad f_{b,0} = \left(1 - \frac{H_{mf}}{H_f}\right)$	
Height of the bed at min. fluid. Velocity	$H_{mf} = H_s \frac{1 - \varepsilon_s}{1 - \varepsilon_{mf}}$	[18]
Height of bed expansion	$H_f = H_{mf} \frac{c_1}{c_1 - c_2}$	
	$C_1 = 1 - \frac{u_{b,0}}{u_{b,avg}} e^{-\frac{0.275}{D_T}}$	
	$C_2 = \frac{u_{b,0}^s}{u_{b,avg}}\left(1 - e^{-\frac{0.275}{D_T}}\right)$	
Gas exchange coefficientBubble to cloud	$K_{bc} = 4.5\left(\frac{u_{mf}}{d_{b,avg}}\right) + 5.85\left(\frac{D_g^{0.5} g^{0.25}}{d_{b,avg}^{5/4}}\right)$	[20]
Cloud to emulsion	$K_{ce} = 6.77\left(\frac{D_g \varepsilon_{mf} u_{b,avg}}{d_{b,avg}^3}\right)^{0.5}$	
Bubble to emulsion mass transfer resistance	$\frac{1}{K_{be}} = \frac{1}{K_{bc}} + \frac{1}{K_{ce}}$	
Binary diffusivities	$D_g = \frac{10^{-3} T^{1.75}\left(\frac{1}{M_{w,i}} + \frac{1}{M_{w,j}}\right)^{\frac{1}{2}}}{P\left[V_{D,i}^{\frac{1}{3}} + V_{D,j}^{\frac{1}{3}}\right]^2}$	[29]

Appendix II. Reaction rate laws and kinetic parameters

Reaction	Stoichiometry and reaction rate equation	Refs.
Methane steam reforming Eq. (1)	$r_{SMR} = \dfrac{k_{SMR}\left(P_{CH_4} P_{H_2O} - \frac{P_{H_2}^3 P_{CO}}{K_{SMR}^{eq}}\right)}{P_{H_2O}^{1.596}}$	[21]
Water gas shift Eq. (2)	$r_{WGS} = \dfrac{k_{WGS}\left(P_{CO} P_{H_2O} - \frac{P_{H_2} P_{CO_2}}{K_{WGS}^{eq}}\right)}{P_{H_2O}}$	
	$k_i = A_i e^{\left(-\frac{E_{act,i}}{RT}\right)}$	

Constant	Value	Unit	
A_{SMR}	$9.74 \cdot 10^4$	mol bar$^{-0.404}$ kg$_{cat}^{-1}$ s^{-1}	[22]
A_{WGS}	$17.2 \cdot 10^2$	Mol bar^{-1} kgcat^{-1} s^{-1}	
$E_{act,SMR}$	$83.6 \cdot 10^3$	J/mol	
$E_{act,WGS}$	$54.53 \cdot 10^3$	J/mol	

References

[1] F. Van Foreest, Perspectives for Biogas in Europe, (2012).

[2] L. Yang, X. Ge, C. Wan, F. Yu, Y. Li, Progress and perspectives in converting biogas to transportation fuels, Renew. Sustain. Energy Rev. 40 (2014) 1133–1152, http://dx.doi.org/10.1016/j.rser.2014.08.008.

[3] J. Xuan, M.K.H. Leung, D.Y.C. Leung, M. Ni, A review of biomass-derived fuel processors for fuel cell systems, Renew. Sustain. Energy Rev. 13 (2009) 1301–1313, http://dx.doi.org/10.1016/j.rser.2008.09.027.

[4] S.D. Angeli, G. Monteleone, A. Giaconia, A.A. Lemonidou, ScienceDirect State-of-the-art catalysts for CH 4 steam reforming at low temperature, Int. J. Hydrogen Energy. 39 (2013) 1979–1997, http://dx.doi.org/10.1016/j.ijhydene.2013.12.001.

[5] F. Gallucci, E. Fernandez, P. Corengia, M. van Sint Annaland, Recent advances on membranes and membrane reactors for hydrogen production, Chem. Eng. Sci. 92 (2013) 40–66, http://dx.doi.org/10.1016/j.ces.2013.01.008.

[6] T. Sato, T. Suzuki, M. Aketa, Y. Ishiyama, K. Mimura, N. Itoh, Steam reforming of biogas mixtures with a palladium membrane reactor system, Chem. Eng. Sci. 65 (2010) 451–457, http://dx.doi.org/10.1016/j.ces.2009.04.013.

[7] A. Iulianelli, S. Liguori, Y. Huang, A. Basile, Model biogas steam reforming in a thin Pd-supported membrane reactor to generate clean hydrogen for fuel cells, J. Power Sources 273 (2015) 25–32, http://dx.doi.org/10.1016/j.jpowsour.2014.09.058.

[8] J.M. Vásquez Castillo, T. Sato, N. Itoh, Effect of temperature and pressure on hydrogen production from steam reforming of biogas with Pd-Ag membrane reactor, Int. J. Hydrogen Energy 40 (2015) 3582–3591, http://dx.doi.org/10.1016/j.ijhydene.2014.11.053.

[9] S. Hara, K. Sakaki, N. Itoh, Decline in hydrogen permeation due to concentration polarization and CO hindrance in a palladium membrane reactor, Ind. Eng. Chem. Res. 38 (1999) 4913–4918, http://dx.doi.org/10.1021/ie990200n.

[10] N. Mori, T. Nakamura, K.I. Noda, O. Sakai, A. Takahashi, N. Ogawa, et al., Reactor configuration and concentration polarization in methane steam reforming by a membrane reactor with a highly hydrogen-permeable membrane, Ind. Eng. Chem. Res. 46 (2007) 1952–1958, http://dx.doi.org/10.1021/ie060989j.

[11] S.H. Volkers, Kuipers Heat Transfer in a Membrane Assisted Bubbling Fluidized Bed with Immersed Horizontal Tubes Heat Transfer in a Membrane Assisted Bubbling Fluidized Bed with Immersed Horizontal Tubes, (2005).

[12] E. Fernandez, A. Helmi, K. Coenen, J. Melendez, J.L. Viviente, D.A. Pacheco, Tanaka, et al., Development of thin Pd–Ag supported membranes for fluidized bed membrane reactors including WGS related gases, Int. J. Hydrogen Energy 40 (2015) 3506–3519, http://dx.doi.org/10.1016/j.ijhydene.2014.08.074.

[13] E. Fernandez, K. Coenen, A. Helmi, J. Melendez, J. Zuñiga, D.A. Pacheco, Tanaka, et al., Preparation and characterization of thin-film Pd–Ag supported membranes for high-temperature applications, Int. J. Hydrogen Energy (2015), http://dx.doi.org/10.1016/j.ijhydene.2015.08.050.

[14] F. Gallucci, M. van Sint Annaland, J.A.M. Kuipers, Autothermal reforming of methane with integrated CO2 capture in a novel fluidized bed membrane reactor. Part 1: experimental demonstration, Top. Catal. 51 (2008) 133–145, http://dx.doi.org/10.1007/s11244-008-9126-8.

[15] S.A.R.K. Deshmukh, J.A. Laverman, A.H.G. Cents, M. Van Sint Annaland, J.A.M. Kuipers, Development of a membrane-assisted fluidized bed reactor. 1. Gas phase back-mixing and bubble-to-emulsion phase mass transfer using tracer injection and ultrasound experiments, Ind. Eng. Chem. Res. (2005) 5955–5965.

[16] K. Kato, C.Y. Wen, Bubble assemblage model for fluidized bed catalytic reactors,

Chem. Eng. Sci. 24 (1969) 1351–1369, http://dx.doi.org/10.1016/0009-2509(69)85055-4.

[17] S.A.R.K. Deshmukh, J.A. Laverman, M. Van Sint Annaland, J.A.M. Kuipers, Development of a membrane-assisted fluidized bed reactor. 2. Experimental demonstration and modeling for the partial oxidation of methanol, Ind. Eng. Chem. Res. (2005) 5966–5976.

[18] S. Mori, C.Y. Wen, Estimation of bubble diameter in gaseous fluidized beds, AIChE J. 21 (1975) 109–115, http://dx.doi.org/10.1002/aic.690210114.

[19] C.-Y. Shiau, C.-J. Lin, Equation for the superficial bubble-phase gas velocity in fluidized beds, AIChE J. 37 (1991) 953–954, http://dx.doi.org/10.1002/aic.690370619.

[20] D. Kunii, O. Levenspiel, Fluidization Engineering, Elsevier, 1991, , http://dx.doi.org/10.1016/B978-0-08-050664-7.50012-3.

[21] T. Numaguchi, K. Kikuchi, Intrinsic kinetics and design simulation in a complex reaction network; steam-methane reforming, Chem. Eng. Sci. 43 (1988) 2295–2301, http://dx.doi.org/10.1016/0009-2509(88)87118-5.

[22] L. Marra, P.F. Wolbers, F. Gallucci, M. van Sint Annaland, Development of a RhZrO2 catalyst for low temperature autothermal reforming of methane in membrane reactors, Catal. Today 236 (2014) 23–33, http://dx.doi.org/10.1016/j.cattod.2013.10.069.

[23] F. Gallucci, M. van Sint Annaland, J. Kuipers, Autothermal reforming of methane with integrated CO2 capture in a novel fluidized bed membrane reactor. Part 2

comparison of reactor configurations, Top. Catal. 51 (2008) 146–157, http://dx.doi.org/10.1007/s11244-008-9127-7.

[24] A. Caravella, G. Barbieri, E. Drioli, Concentration polarization analysis in self-supported Pd-based membranes, Sep. Purif. Technol. 66 (2009) 613–624, http://dx.doi.org/10.1016/j.seppur.2009.01.008.

[25] F. Gallucci, M. Van Sint Annaland, J.A.M. Kuipers, Theoretical comparison of packed bed and fluidized bed membrane reactors for methane reforming, Int. J. Hydrogen Energy, Elsevier Ltd, 2010, pp. 7142–7150, , http://dx.doi.org/10.1016/j.ijhydene.2010.02.050.

[26] A.L. Zydney, Stagnant film model for concentration polarization in membrane systems, J. Membr. Sci. 130 (1997) 275–281, http://dx.doi.org/10.1016/S0376-7388(97)00006-9.

[27] A. Helmi, R.J.W. Voncken, A.J. Raijmakers, I. Roghair, F. Gallucci, M. van Sint Annaland, On concentration polarization in fluidized bed membrane reactors, Chem. Eng. J. 332 (2018) 464–478, http://dx.doi.org/10.1016/j.cej.2017.09.045.

[28] H. Amandusson, L.G. Ekedahl, H. Dannetun, Effect of CO and O2 on hydrogen permeation through a palladium membrane, Appl. Surf. Sci. 153 (2000) 259–267, http://dx.doi.org/10.1016/S0169-4332(99)00357-8.

[29] E.N. Fuller, P.D. Schettler, J.C. Giddings, A new method for prediction of binary gas-phase diffusion coefficients, Ind. Eng. Chem. 58 (1966) 18–27, http://dx.doi.org/10.1021/ie50677a007.